Dynamic Simulation of a PEM Electrolysis System

Markus Pollak[1] André Thüring[1] Wilhelm Tegethoff[1,2]

[1]TLK-Thermo GmbH, Germany, {m.pollak, a.thuering}@tlk-thermo.com
[2]Institut für Thermodynamik, Technische Universität Braunschweig, Germany,
{w.tegethoff}@tu-braunschweig.de

Abstract

Electrolysis systems are the key technology to produce hydrogen from renewable energy sources. The modeling and simulation of proton exchange membrane (PEM) electrolyzers and the connected power grid present challenges due to highly fluctuating capacities in the available electrical power. Our study focuses on the modeling of the electrolyzer and its balance of plant with varying power supply resulting from renewable energy sources. The balance of plant contains a water supply system, the electrical power supply and processes for treating the produced hydrogen, in particular drying. The electrolyzer model is validated using steady-state and dynamic data from the literature and it is shown that the developed model accurately represents those measurement results. Furthermore, we implement an empirical degradation model to assess the effects of different use-cases on the efficiency of the electrolyzer.

Keywords: PEM electrolysis, hydrogen, dynamic simulation, two-phase flow, degradation

1 Introduction

A water electrolyzer is a device that is used to split water into hydrogen and oxygen using electrical energy. The production of hydrogen is essential for the chemical industry, because it is the feedstock of many processes. Moreover, hydrogen is also widely discussed as a future energy carrier (Hancke, Holm, and Ulleberg 2022; Hou and Yang 2024). To produce hydrogen in a sustainable way, the combination of electrolyzer and renewable energy sources is the key (Hou and Yang 2024; Reimann, Kohlenbach, and Röntzsch 2023). The operation characteristics of renewable energy sources, such as wind energy farms and photovoltaics, are inherently dynamic. Therefore, an electrolyzer connected to a power grid with a large share of renewable energy sources should be able to handle dynamic capacities.

There are various water electrolyzer technologies on the market, each with specific properties. Our study focuses on proton exchange membrane (PEM) electrolyzers because of the following arguments. This type of electrolyzer is able to operate dynamically due to its low temperature requirements. As well, low operating temperatures allow for a fast start-up. A further advantage of the PEM electrolyzer is that it can be operated at high pressures and therefore reduces the power required to compress hydrogen for storage applications (Hancke, Holm, and Ulleberg 2022).

To assess the performance of different electrolyzers or design an electrolzyer for a specific application, detailed simulation models are needed. Electrolyzers are generally operated in combination with other systems of various engineering disciplines. Therefore, the use of Modelica as a modeling language is ideal as many Modelica libraries focusing on the modeling of energy system are available and can be used to investigate future energy systems.

PEM electrolyzer models with different levels of detail have been published in the literature (Engel et al. 2025; Hancke, Holm, and Ulleberg 2022; Reimann, Kohlenbach, and Röntzsch 2023; Krenz et al. 2024). A novelty of our approach presented in this work is that we combine a detailed physics-based electrolyzer system model with an empirical degradation model published by (Schofield et al. 2025).

In the current study, an electrolyzer is investigated under steady-state and dynamic operating conditions. To assess the effects of fluctuating power supply on the efficiency and degradation of an electrolyzer, the electrolyzer is connected to a wind turbine as a power supply and meteorological data are used to generate operation profiles. The combination of an electrolyzer with a renewable energy source is arguably a relevant use case for hydrogen production in the future.

In the following section, the working principle and the main features of the PEM electrolyzer are introduced. The third section discusses the function and modeling of the specific components selected to build the electrolyzer system model. In the fourth section, we focus on the simulation of steady-state and dynamic operation and study the predicted degradation. The results obtained are compared with data from the literature.

2 PEM Electrolyzer Model for System Simulations

The PEM electrolyzer model discussed in this study was developed using the commercially available Modelica libraries TIL, TILMedia and the TIL3_Addon_HydrogenEnergySystems each in version 2025.1 (TLK-Thermo GmbH 2024). Dymola 2024x is used as modeling and simulation environment

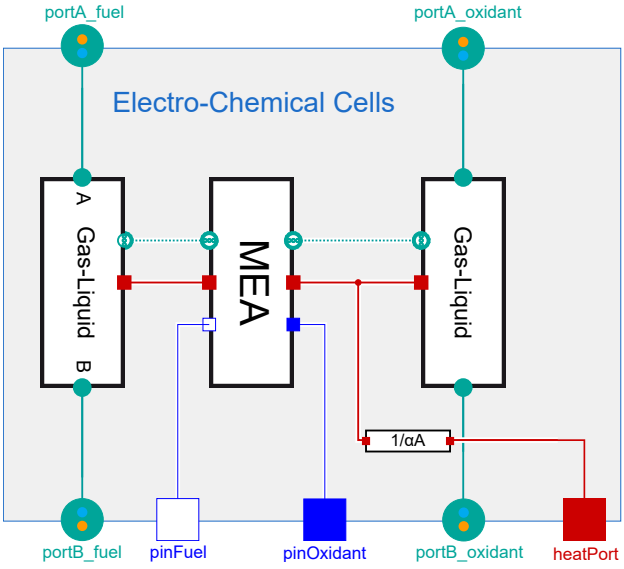

Figure 1. Structure of the stack model divided into fuel and oxidant channels and a membrane electrode assembly. Turquoise lines represent mass transfer. Dashed lines symbolize diffusive mass transfer and full lines convective mass transport. Heat transfer is marked by red lines and electrical current by blue lines.

(Dassault Systèmes SE 2024). A novelty of our approach is to combine a physics-based model with an empirical degradation model to assess the effects of degradation in realistic operating scenarios. The electrolyzer model is divided into three subdomains representing the fuel channel, the membrane electrode assembly (MEA) and the oxidant channel, as shown in Fig. 1. To calculate spatially resolved results, the model is divided into smaller discretization elements in the flow direction, but keeping the structure given in the figure. This way, the local formation and transport of product gases and water can be observed. To simulate a full stack consisting of multiple cells, one representative cell is simulated in detail and the results scaled-up by multiplying the results of the single cell by the number of cells in the stack, as described by (Tang 2016) for a fuel cell.

2.1 Electrochemical Foundation and Balances

To describe the operation of an electrolyzer, we start by introducing the relevant balance equation, and then we derive the most important metrics of the electrolyzer. On the oxidant side of the electrolyzer, water is supplied to the stack oxidant port A, as shown in Fig. 1. As typical for PEM electrolyzers, water is supplied to the anode channels of the electrolyzer only. Because the membrane is permeable to water, water is transported towards the cathode, as described in the next section. On the anode electrode water is split up into protons and oxygen:

$$\text{Anode}: \quad \mathrm{H_2O} \rightarrow 2\mathrm{H^+} + 2\mathrm{e^-} + \frac{1}{2}\mathrm{O_2} \tag{1}$$

On the cathode, protons and electrons form hydrogen molecules:

$$\text{Cathode}: \quad 2\mathrm{H^+} + 2\mathrm{e^-} \rightarrow \mathrm{H_2} \tag{2}$$

In summary, the overall reaction reads:

$$\mathrm{H_2O} \rightarrow \mathrm{H_2} + \frac{1}{2}\mathrm{O_2} \tag{3}$$

The products and water leave the system at the fuel port B and oxidant port B. Heat can be removed using a heat port. In the electrolyzer, a two-phase flow is typical since the water is supplied in liquid state and the products are gases. To split water into oxygen and hydrogen, electrical power must be supplied to the electrolyzer. The calculation of the required electrical power is described in the following paragraph. In the model, the current is supplied directly to the MEA as shown in Fig. 1.

To derive the minimal power required for the electrolysis, a steady-state operation is assumed in the following equations, but the model is formulated for dynamic operation. The following mass balance holds for the electrolyzer:

$$\dot{m}_{\mathrm{H_2O,in}} - \dot{m}_{\mathrm{H_2O,out}} - \dot{m}_{\mathrm{H_2,out}} - \dot{m}_{\mathrm{O_2,out}} = 0 \tag{4}$$

The first law of thermodynamics for the electrolyzer reads:

$$\dot{H}_{\mathrm{H_2O,in}} - \dot{H}_{\mathrm{H_2O,out}} - \dot{H}_{\mathrm{H_2}} - \dot{H}_{\mathrm{O_2}} + \dot{Q} + P = 0 \tag{5}$$

The second law of thermodynamics is stated as follows:

$$\dot{S}_{\mathrm{H_2O,in}} - \dot{S}_{\mathrm{H_2O,out}} - \dot{S}_{\mathrm{H_2}} - \dot{S}_{\mathrm{O_2}} + \frac{\dot{Q}}{T} = \dot{S}_{\mathrm{prod}} \tag{6}$$

We assume an isobaric and isothermal reaction, so that the reactants and products have the same pressure and temperature.

Combing the first and the second law results in a new equation:

$$\dot{G}_{\mathrm{H_2O,in}} - \dot{G}_{\mathrm{H_2O,out}} - \dot{G}_{\mathrm{H_2}} - \dot{G}_{\mathrm{O_2}} + P = T\dot{S}_{\mathrm{prod}} \tag{7}$$

Here, the relation for the Gibbs free energy is used:

$$G = H - TS \tag{8}$$

A special relation holds when no entropy is produced: The minimum work needed to split a water molecule is given by the Gibbs free energy of the reaction ΔG_R:

$$\Delta G_R = \Delta H_R - T\Delta S_R \tag{9}$$

It is the difference of the reaction enthalpy ΔH_R and the product of the cell temperature T and reaction entropy ΔS_R. The terms of the equation are explained below. The Gibbs free energy of the reaction can be directly linked

DOI
10.3384/ecp218413

to the voltage between the electrodes using the number of transferred electrons z and the Faraday constant F:

$$U_{\text{rev}} = -\frac{\Delta G_R}{zF} \tag{10}$$

The Gibbs free energy of the reaction depends on the temperature, the pressure and the composition of reactants supplied to the electrolyzer.

Another important voltage, the so-called thermoneutral voltage, can be derived from the reaction enthalpy:

$$U_{\text{TN}} = -\frac{\Delta H_R}{zF} \tag{11}$$

When operated at this voltage an adiabatic electrolyzer will operate at constant temperature (Bernt 2019), assuming no temperature gradients in the electrolyzer. Otherwise, the reversible heat of the reaction leads to a change in the cell temperature. The reversible heat is calculated using the electrical current and the thermoneutral and reversible voltages:

$$\dot{Q}_{\text{rev}} = I(U_{\text{rev}} - U_{\text{TN}}) \tag{12}$$

In addition to the reversible heat, the losses occurring in an operating cell produce irreversible heat flows. Those losses are directly related to the entropy production rates, as presented by (Struchtrup 2014). The major losses to be considered in an electrolyzer cell are activation, Ohmic, and mass transfer losses and are introduced in the following section.

2.2 Electrochemical Transport Models

In the following, the transport in the MEA is presented. The water content λ_{W} represents the amount of water in the membrane according to (Springer, Zawodzinski, and Gottesfeld 1991). In the electrolyzer, the membrane is always equilibrated with liquid water on the oxidant side and therefore water content is assumed to be constant according to (Springer, Zawodzinski, and Gottesfeld 1991):

$$\lambda_{\text{W}} = 22 \tag{13}$$

The proton conductivity of the membrane is directly affected by its water content and is modeled as stated by (Springer, Zawodzinski, and Gottesfeld 1991):

$$\sigma_{\text{mem}} = (0.5139\lambda_{\text{W}} - 0.326)\exp\left(1268\,\text{K}\left(\frac{1}{303\,\text{K}} - \frac{1}{T}\right)\right) \tag{14}$$

Using the proton conductivity σ_{mem}, the membrane thickness δ_{mem} and the active area A, the electrical resistance of the proton conduction can be calculated:

$$R_{\text{mem}} = \frac{\delta_{\text{mem}}}{\sigma_{\text{mem}} A} \tag{15}$$

The irreversible voltage loss is then calculated by the following relation:

$$\Delta U_{\text{ohm}} = R_{\text{mem}} I \tag{16}$$

The activation loss is calculated using a Tafel equation with the parameters crossover current density i_{X} and the exchange current density i_0:

$$\Delta U_{\text{act}} = \frac{RT}{\alpha z F}\log\left(\frac{i + i_{\text{X}}}{i_0}\right) \tag{17}$$

Since the losses on the fuel side are comparatively small, they are neglected and only the oxidant side is considered.

Furthermore, the mass transfer losses are accounted for employing a limiting current density of $i_L = 6\,\text{A/cm}^2$ (Crespi et al. 2023):

$$\Delta U_{\text{conc}} = \frac{RT}{\alpha z F}\log\left(\frac{i_L}{i_L - i}\right) \tag{18}$$

The degradation of electrolzyer cells during operation is a current topic of research and of great importance when addressing economic viability questions. In the literature, different models for catalyst and membrane degradation can be found. A major drawback of the currently published models is their high computational demand. Therefore, an empirical model fitted by (Schofield et al. 2025) is implemented in the electrolyzer model.

$$\frac{d\Delta U_{\text{deg}}}{dt} = \begin{cases} 30\,\mu\text{V/h} & \text{if } 0 < i < 1\,\text{A/cm}^2 \\ 30\,(\mu\text{V cm}^4)/(\text{A}^2\,\text{h})\,[i(t)]^2 & \text{otherwise} \end{cases} \tag{19}$$

The data used for the calibration of the degradation model originate from accelerated stress tests and, therefore, might overpredict the rate of degradation under real operating conditions.

The cell voltage is then calculated using the losses ΔU introduced before and the reversible cell voltage U_{rev}:

$$U_{\text{cell}} = U_{\text{rev}} + \Delta U_{\text{ohm}} + \Delta U_{\text{act}} + \Delta U_{\text{conc}} + \Delta U_{\text{deg}} \tag{20}$$

With the cell voltage, the heat release from the reaction can be calculated:

$$\dot{Q} = I(U_{\text{cell}} - U_{\text{TN}}) \tag{21}$$

The main functions of the membrane in the electrolyzer are proton conduction, electric insulation and separation of the species. However, a real membrane is not fully impermeable to the species in the electrolyzer. Therefore, both the produced gases and water can partially travel through the membrane. The transport of the produced gases is driven by a partial pressure difference, while the transport of water occurs due to an absolute pressure gradient and because of electro-osmotic drag (EOD).

The permeation is modeled with the following equation and using parameters published by (Ahluwalia and Wang 2007) :

$$\dot{n}_{\text{drag,i}} = \frac{K_i A}{\delta_{\text{mem}}}\Delta p_i \tag{22}$$

For the calculation of the EOD, a constant drag coefficient $\varepsilon_{\text{EOD}} = 2.5$ is used (Ma et al. 2021). The water transfer is then calculated using the electric current:

$$\dot{n}_{\text{EOD}} = \frac{\varepsilon_{\text{EOD}} I}{F} \tag{23}$$

The heat produced by the reaction is transported to the fluid channels as described in the next section.

2.3 Fluid Channels

Fluid channels are required to supply the anode with water and remove reaction products from the electrolyzer. The channels are connected to both sides of the MEA as shown in Fig. 1. The electrochemical reaction produces gaseous products that mix with liquid water on the anode side. Therefore, it is necessary to consider two-phase flow characteristics when modeling the flow inside the fluid channels. In this study, we use a phase-separate modeling approach that allows us to model a thermal and chemical non-equilibrium of the gas and liquid phases. The relevant equations for describing the flow in the electrolyzer are outlined below.

First, the most important quantities of the two-phase flow are introduced. The void fraction is defined as the volume ratio of gas and total volume:

$$\varepsilon = \frac{V_g}{V} \tag{24}$$

The overall volume is the sum of the volumes occupied by gas and liquid phases:

$$V = V_g + V_l \tag{25}$$

The mass balance for the gas phase, denoted by the index g, is given by the following relation:

$$\varepsilon \frac{d\rho_g}{dt} V - \rho_g \frac{dV_l}{dt} = \dot{m}_{g,in} + \dot{m}_{g,out} + \dot{m}_{PC} + \sum \dot{m}_{MT,g,i} \tag{26}$$

Here, the time derivative of the liquid volume is given by

$$\frac{dV_l}{dt} = \beta \frac{dT}{dt} \frac{m_l}{\rho_l} + \frac{1}{\rho_l} \frac{dm_l}{dt} \tag{27}$$

with β being the isobaric expansion coefficient. Using a smooth limiter, it is always guaranteed that small amounts of liquid and gas phase are present in each control volume to avoid singularity.

Using an explicit formulation of time derivative of the density avoids symbolic manipulation of the equation system and thereby simplifies the solution (Richter 2008):

$$\frac{d\rho}{dt} = \left(\frac{d\rho}{dh}\right)_{p,\xi} \frac{dh}{dt} + \left(\frac{d\rho}{dp}\right)_{h,\xi} \frac{dp}{dt} + \left(\frac{d\rho}{d\xi}\right)_{p,h} \frac{d\xi}{dt} \tag{28}$$

For the liquid phase the mass balance reads:

$$\frac{dm_l}{dt} = \dot{m}_{l,in} + \dot{m}_{l,out} - \dot{m}_{PC} + \dot{m}_{MT,l} \tag{29}$$

Both equations are explicitly coupled by a possible phase change given by the common term $\dot{m}_{PC}$.

For the pressure calculation, a mechanical equilibrium of both phases is assumed:

$$p_g = p_l \tag{30}$$

The pressure is derived from the gas phase. The momentum balance is formulated in steady-state.

The gas phase consists of a mixture of hydrogen, oxygen and water vapor.

$$\begin{aligned} m_g \frac{d\xi_i}{dt} = {} & (\xi_{i,in} - \xi_i)\dot{m}_{g,in} + (\xi_{i,out} - \xi_i)\dot{m}_{g,out} \\ & + (\xi_{\text{condensed,i}} - \xi_i)\dot{m}_{PC} + \xi_i \dot{m}_{MT,g,i} \end{aligned} \tag{31}$$

Here, the mass fraction vector $\xi_{\text{condensed,i}}$ contains zeros except for a one at the position representing water. Since the liquid phase consists of water as one pure species in the model only, no explicit formulation of the species balance is required for the liquid.

The energy balance is formulated for each phase separately. However, for the current study, a thermal equilibrium is assumed:

$$T_g = T_l \tag{32}$$

For the gas phase, the energy balance reads:

$$\begin{aligned} m_g \frac{dh_g}{dt} = {} & (h_{g,in} - h_g)\dot{m}_{g,in} + (h_{g,out} - h_g)\dot{m}_{g,out} + (h_l - h_g)\dot{m}_{PC} \\ & + \sum (h_{i,MT} - h_g)\dot{m}_{MT,g,i} + \dot{Q} + \varepsilon V \frac{dp}{dt} \end{aligned} \tag{33}$$

The liquid phase energy balance is as follows:

$$\begin{aligned} m_l \frac{dh_l}{dt} = {} & (h_{l,in} - h_l)\dot{m}_{l,in} + (h_{l,out} - h_l)\dot{m}_{l,out} - (h_l - h_g)\dot{m}_{PC} \\ & + (h_{MT} - h_l)\dot{m}_{MT,g,i} + \dot{Q} \end{aligned} \tag{34}$$

The heat transfer from fluid to membrane and the bipolar plate is calculated using a temperature difference and a fixed heat transfer coefficient:

$$\dot{Q} = \alpha A \Delta T \tag{35}$$

For the forced convection a constant heat transfer coefficient of $\alpha = 2000\,\mathrm{W/(m^2K)}$ is used, reflecting that the exact geometry of the channels in the bipolar plate is unknown. Furthermore, the heat loss to the environment is calculated using the stack surface area and the heat transfer correlations for free convection from the literature (Klan and Thess 2013). The heat transfer area was calculated according to (Tjarks 2017).

Analogously to heat transfer, the mass transfer processes are calculated using a mass transfer coefficient and a concentration difference.

$$\dot{m} = \beta A \Delta c \tag{36}$$

The interface mass transfer of water is driven by a concentration difference between actual and saturated state:

$$\dot{m}_{\text{PC}} = \beta_{\text{PC}} A (c_{\text{sat}} - c) \tag{37}$$

To simplify the calculation, an ideal transport can be assumed, whereby the concentration c and the saturation concentration c_{sat} are set equal. Due to intense mixing, the produced gases are typically saturated with water.

DOI
10.3384/ecp218413

3 Electrolyzer System Model

The modeled electrolyzer system is shown in Fig. 2. To produce hydrogen of defined quality in a PEM electrolyzer, a water supply system, an electrical connection to a power supply, and a hydrogen treatment system are necessary. The modeled hydrogen treatment system consists of two drying stages, thermal drying and adsorptive drying, followed by a compressor. In the following, the subsystems and their specifications are discussed in detail.

Stack

An electrolyzer previously analyzed in the literature (Crespi et al. 2023) is modeled and simulated in this work. A summary of the most relevant stack parameters is given in Table 1. Two separators are directly connected to the stack to remove liquid water from the gas flows on fuel and oxidant side. On the oxidant side, the removed water is fed to the liquid loop again. The oxygen produced by the electrolyzer is released to the environment. On the fuel side, further treatment of the liquid water was not modeled. However, the produced hydrogen gas, which is typically moisture-laden, undergoes further treatment in the subsequent steps.

Table 1. Parameters of the modeled electrolyzer stack.

Quantity	Symbol	Unit	Value
Nominal Current	I	A	410
Nominal Power	P_{el}	kW	60
Number of cells	n_{C}	1	65
Active Area	A_{MEA}	cm^2	214
Membrane Thickness	δ_{mem}	mm	0.322
Thermal Capacity	C_{Stack}	kJ/K	155.0

Water Supply and Cooling Loop

The water supply system circulates water in the cathode loop and feeds to the electrolyzer to replace water consumed by the electrochemical reaction. In addition, the circulated water is employed for the thermal management of the electrolyzer. Therefore, a chiller is integrated into the water loop that can reject heat to a cooling circuit. In addition, a storage tank is included to buffer water consumption and act as a thermal capacity. To refill water a pump is modeled. The supply water is assumed to be deionized.

Hydrogen Treatment System

The purification unit consists of two different drying processes. In the first step, water is removed from the produced hydrogen by lowering its temperature below the saturation point using a heat exchanger connected to a cooling circuit. In order to fulfill the typically strict requirements for the hydrogen purity, an adsorptive drying process is implemented downstream of the thermal drying process. In this study, a temperature swing adsorption (TSA) system is modeled as suggested by (Tjarks et al. 2018) using the TIL Adsorption Library (TLK Energy GmbH 2024). The TSA system consists of two adsorbers that are operated alternately. Both adsorbers are filled with Zeolith as an adsorbent (Tjarks et al. 2018). When hydrogen is produced, one adsorber is used to remove water from the fuel gas. The adsorption process is driven by a gradient in the chemical potential of water in the fuel gas and adsorbed water. During operation, water accumulates in the adsorber until it reaches a defined loading state. When this loading state is reached, the adsorbers are switched and the adsorber that was in the drying operation is then regenerated using a recirculation system. In the recirculation loop, hydrogen is heated up to 160 °C then enters the adsorber and gets humidified inside. A blower is used to recirculate hydrogen with a defined flow rate. The water is removed from the hydrogen after leaving the adsorber by lowering the temperature of hydrogen below its saturation point using the environment or a cooling circuit as the heat sink. To switch between the two adsorbers, eight control valves are utilized.

After the purification stages, hydrogen is compressed to a defined level. This step is necessary to increase the volumetric energy density of hydrogen.

While the electrolyzer is modeled in detail as described above, the pumps and compressors are modeled with constant efficiencies. For the heat exchangers, a finite-volume-approach was employed (Richter 2008). The heat transfer coefficients are assumed to be constant. In addition, a constant separation efficiency is assumed in the water separator models shown in Fig. 2. All efficiencies and other significant parameters are summarized in Table 2. The pressure levels and the nominal coolant flow rate are adjusted according to (Crespi et al. 2023).

Table 2. Parameters of the component models in the electrolyzer system.

Quantity	Symbol	Unit	Value
Compressor Efficiency	$\eta_{\text{comp,isen}}$	1	0.7
Recirculation Blower	$\eta_{\text{b,isen}}$	1	0.4
Pump Efficiency	P_{el}	kW	0.97
Separator Efficiency	η_{sep}	1	0.99
Hydrogen Storage Pressure	p	bar	200
Cathode Pressure	p	bar	30
Anode Pressure	p	bar	3.5
Volume Tank	V	L	200
Nominal Coolant Flow Rate	$\dot{m}$	kg/s	0.63
Heat Transfer Resistance			
Chiller	R_{th}	K/W	0.001
Condenser	R_{th}	K/W	0.003
Heater	R_{th}	K/W	0.003

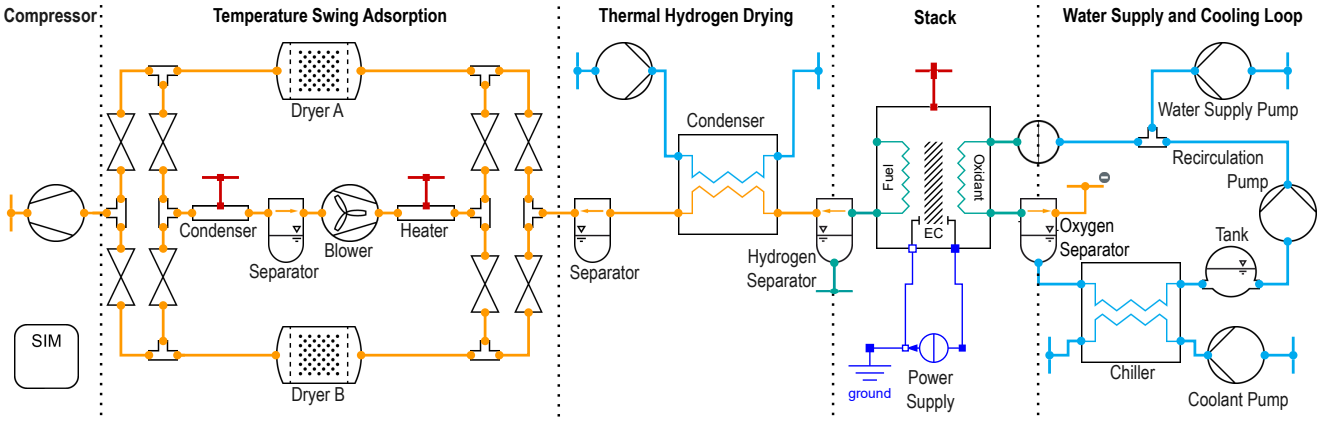

Figure 2. Electrolyzer with its main supply and hydrogen purification systems. Gas connections are colored in orange, liquid in blue, two-phase flow in turquoise and electrical current in dark blue. Heat flows are represented by red lines.

4 Steady-State and Dynamic Operation of PEM Electrolyzer

This section provides an overview of the simulation results obtained with the proposed model. First, steady-state operation and calibration of the stack are discussed. Next, dynamic operation scenarios are investigated. Finally, the degradation of the stack during dynamic operation is explored.

4.1 Steady-State Operation

Data from the literature data published by Crespi et al. (2023) is used to calibrate and validate the model discussed in the previous section. The operating conditions are given in Table 2. First, the geometry of the model is adjusted according to the data given in the paper of Crespi et al. (2023) also shown in Table 1. Next, a calibration is performed using steady-state measurement data of the same publication recorded at different operating temperatures and current densities. Data used to validate the model are not used in the fitting process.

The exchange current density $i_0 = 1.05 \times 10^{-7}\,\mathrm{A/cm^2}$, the effective membrane thickness $\delta_{\mathrm{mem,eff}} = 455\,\mu\mathrm{m}$ and the crossover current density $i_X = 0.02\,\mathrm{A/cm^2}$ have been used in a fitting process to obtain an accurate representation of the electrolyzer data published by Crespi et al. (2023) . Only data for an operating temperature of 50 °C were used for the fitting. The other part of the data, at operating temperatures of 45 °C and 60 °C, were used for validation.

In Fig. 3, the results of the calibration and validation can be found. Overall, the model accurately reflects the measurement data. The highest deviation between the measurement and the simulations is observed for small current densities. The mean absolute deviation is 0.013 V for all simulated operating points. The maximum deviation between simulation and measurement is 0.035 V .

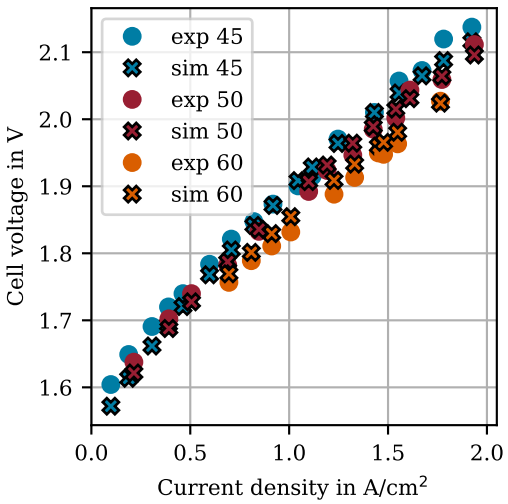

Figure 3. Comparison of measured and simulated voltages at different temperatures and current densities. The other operating conditions are set according to Table 2.

4.2 Dynamic Operation

One application of a PEM electrolyzer is the direct connection to a renewable energy source, such as a wind farm. Renewable energy sources such as wind and photovoltaics are highly fluctuating due to the weather conditions at the location of the electrolyzer. The aim of this section is to investigate whether the developed model can accurately simulate the response of the electrolyzer to a time-varying power supply. First, the calibration of the thermal capacity of the cooling circuit is conducted. Next, the gas volumes on the fuel side are calibrated and the pressure build-up investigated. Finally, the dynamic operation is studied with regard to efficiency, safety and degradation of the electrolyzer.

Warm-Up of the Electrolyzer

For an electrolyzer connected to a renewable and weather-dependent energy source, it is important to see how fast it can reach the desired operating temperature and produce

DOI 10.3384/ecp218413

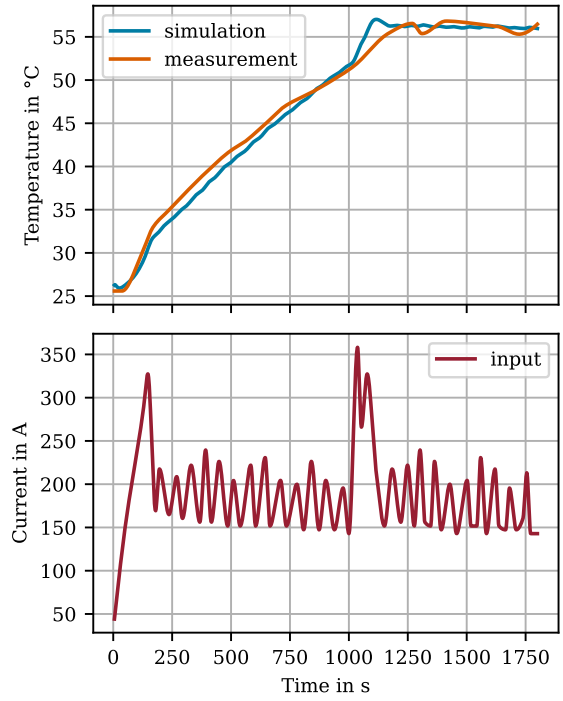

Figure 4. Comparison of simulated and measured temperatures during start-up and operation of the electrolyzer with varying current input with an average of I = 188 A.

hydrogen with high efficiency. In the work of Crespi et al. (2023), the warm-up of an electrolyzer system under given power capacity profiles is shown. The heat produced in the electrochemical reaction is utilized to warm up the electrolyzer from ambient temperature. The measurements are shown in Fig. 4. A mean current of 188 A is supplied to the electrolyzer. During warm-up the pump in the cooling circuit is deactivated so that no heat is drawn from the system. The amount of heat produced by the reaction depends on the voltage of the cell and thereby on the current supplied to the electrolyzer. The warm-up scenario measured by Crespi et al. (2023) is used in this study to calibrate the model parameters. The adjusted parameter is the water mass in the cooling circuit.

The results of the measurement and the simulation with different parameter values for the water mass are shown in Fig. 4. A steady-state is reached after about 1100 s. In the electrolyzer simulation results, it becomes obvious that the mass of water has a significant influence on the warm-up process due to the high heat capacity of water. The water mass in the liquid loop is adjusted to 50 kg in the calibration process.

The simulation of another warm-up cycle is shown in Fig. 5. Compared to the warm-up shown in Fig. 4, the average current supplied to the electrolyzer is 211 A. A quasi-steady-state temperature is reached after approximately 800 s after the start-up, both in simulation and measurement. In addition to the temperature curve, a comparison of the simulated and measured cathode pressures is shown over time. A total volume of 9.5 L was assumed for

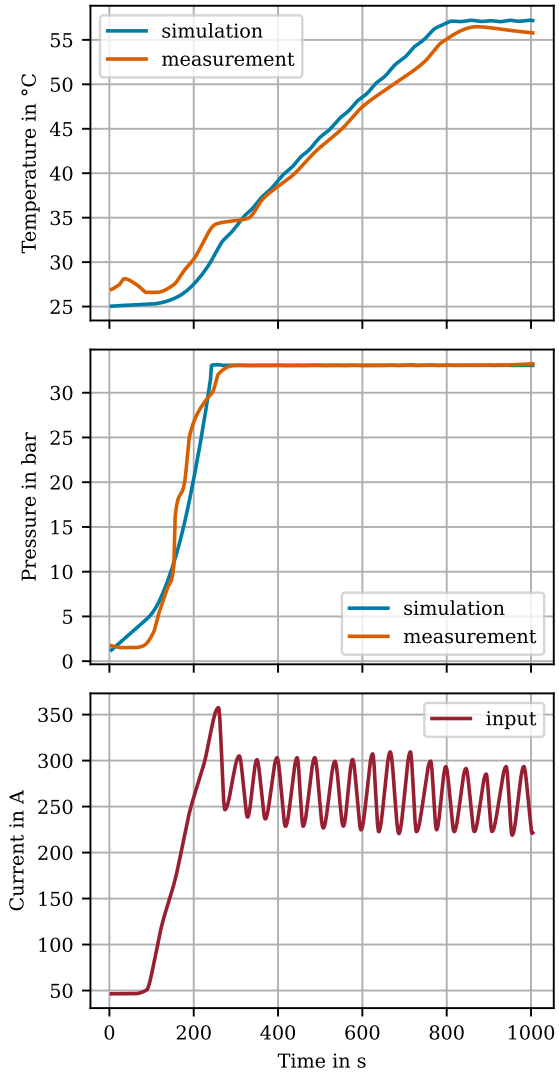

Figure 5. Comparison of simulated and measured temperatures during start-up and operation of the electrolyzer with varying current input with an average of I = 211 A. Simulated and measured pressure build-up are also shown.

the gas on the fuel side of the electrolyzer. The pressure build-up is predicted to be more uniform by the simulation model than in the measurement. In the curve representing the measurement, different slopes are visible that cannot be linked to the input of the current density. In particular, the pressure plateau at the beginning of the recorded data does not appear to be in agreement with the input current. However, quasi-steady-state of the cathode pressure is reached in measurement and simulation after about 240 s.

Electrolyzer Connected to a Wind Turbine

As future energy systems become more dynamic, flexibility in operation is crucial to adapt to fluctuating demands and decentralized production.

In order to operate the electrolyzer model with a dynamic electrical power supply, the scenario of a wind turbine is selected. Therefore, a power supply profile is cre-

ated on the basis of wind data from the DWD for Braunschweig (German Meteorological Service (DWD) 2025). The hourly data indicate the wind speed at ground level. For the calculation of the electrical power generation by the wind turbine, a simplified approach is employed based on (Heier 2022). The wind turbine has a hub height of 45 m and a rotor diameter of 44 m. Using the simplified model, the hourly electrical power supply from the wind turbine to an electrolyzer is calculated for one week in March 2023. The ambient temperature is set to $T_{\text{amb}} = 8\,^{\circ}\text{C}$, which is the average for this month.

Table 3. Electrolysis system simulation results for a week of operation in March 2023 for an electrolyzer with and without grid connection.

Quantity	Symbol	Unit	Value
With Grid Connection			
Hydrogen Produced	m_{H_2}	kg	83.51
Electrical Energy Consumption	E_{el}	kWh	4534.9
Average Efficiency	η	1	0.6138
Without Grid Connection			
Hydrogen Produced	m_{H_2}	kg	79.9
Electrical Energy Consumption	E_{el}	kWh	4367.59
Average Efficiency	η	1	0.6097

To study the effect of different operation strategies, we analyzed two scenarios in terms of the efficiency that can be achieved and the amount of hydrogen that can be produced. For the first scenario, a grid connection of the electrolyzer is assumed. If the available power from the wind turbine falls below 5 kW, it is assumed that the electrolyzer operates at a minimum power that is supplied by the electrical grid. This power is the minimum to keep the electrolyzer at operating temperature. In the second scenario with no grid connection, the electrolyzer is turned off if the available electrical power from the wind turbine falls below a 1 kW threshold. As a result, the electrolyzer temperature decreases due to heat losses to the cold environment. In both scenarios, the maximum power is limited to 60 kW.

The simulation results of both operation scenarios are plotted in Fig. 6. In the figure, the stack temperature, the hydrogen production rate, and the power supply are plotted against time. In the stack temperature, differences are visible in the times when no electrical power is available from the wind turbine. Large temperature decreases can be seen during times when no power is supplied by the wind turbine. The grid-connected electrolyzer remains at an operating temperature of roughly 50 °C due to the additional power supplied by the grid. In both hydrogen production and in the power supply, the effect of the grid connection is shown as an offset when there is no electricity from the wind turbine.

To calculate the efficiency of the system, the hydrogen production rate is integrated and multiplied by the lower heating value (LHV) of hydrogen $\text{LHV}_{\text{H}_2} = 120\,\text{MJ/kg}$. The result is then divided by the time integral of electrical power consumed by the stack, pumps, blower and compressor. This yields the efficiency of the system:

$$\eta = \frac{m_{\text{H}_2}\,\text{LHV}_{\text{H}_2}}{E_{\text{el}}} \tag{38}$$

The integral results of the calculated scenarios are summarized in Table 3. Due to the energy supplied by the grid, which is used when no electricity is available from the wind turbine, the hydrogen production of the grid-connected electrolyzer system is about 4.5 % higher than the electrolyzer without a grid connection. For the same reason, the electrical energy consumption of the grid-connected system is also higher. Moreover, the efficiency of the grid-connected system is higher. This is because hydrogen production at low current densities is very efficient and on the other hand the grid-connected electrolyzer benefits from higher operating temperatures, where operation is slightly more efficient.

Furthermore, the simulated results of the hydrogen concentration on the oxidant side were monitored to check if the flammability limit of hydrogen in oxygen is exceeded at certain operating points. The hydrogen concentration on the oxidant side depends on the permeation and the recirculation rate. It could be observed in the simulation results that the hydrogen concentrations on the anode are higher for the electrolyzer without a grid connection. In the case of the electrolyzer without grid connection, the flammability limit is exceeded at times when the power is reduced rapidly. As a result, countermeasures would have to be taken. For the grid-connected electrolyzer, the limit is never exceeded. Generally, for an accurate description of the transient accumulation of hydrogen during operation, the model needs further parameters, such as volumes of components and materials.

The simulation times for both the grid-connected and the non-connected electrolyzer scenario shown in Fig. 6 are about 75 s on a laptop equipped with an Intel i7-1360P processor.

Prediction of the Degradation in the Electrolyzer

An empirical degradation model (eq. 19) published for the PEM electrolyzer was implemented in the electrolyzer model. To assess the degradation predicted by the empirical model, the simulation of the electrolyzer connected to the wind turbine was conducted again, but for the entire period of March 2023. The grid-connected electrolyzer was selected due to its higher efficiency.

After one month of simulated operation, the voltage of an average single cell in the electrolyzer stack increased by approximately 0.045 V. Extrapolating this result over a period of the year would result in an increase of voltage

DOI
10.3384/ecp218413

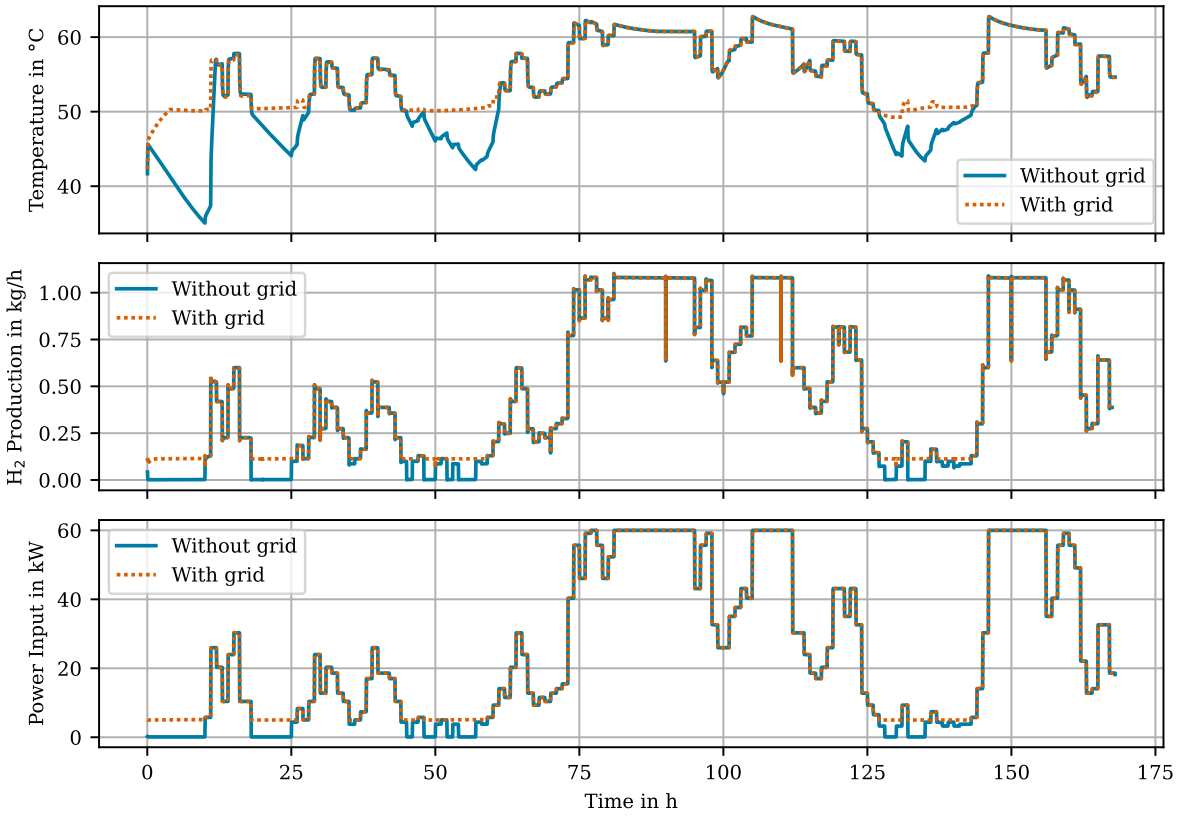

Figure 6. Simulation results of a 60 kW electrolyzer connected to a wind turbine with and without connection to the electric grid. The operating temperature, hydrogen production and power input of both scenarios are compared for the first week of March 2023.

by 0.54 V per single cell. When comparing this extrapolated result to the operating voltages published by (Crespi et al. 2023), the increase of voltage due to degradation would lower the efficiency drastically. In comparison to irreversible degradation results published by (Krenz et al. 2024), the degradation rates reported here for the electrolyzer model are high and result from the fact that irreversible and reversible degradation are not separated in the model. More detailed degradation models are reported in the literature and might help to improve the predictions (Rakousky 2016; Krenz et al. 2024).

The obtained result also demonstrates how important dynamic physics-based simulation models are to check the plausibility of calculated degradation results and to verify degradation models developed using lab-scale electrolyzers. In particular, the ability of physics-based simulation models to study realistic operating scenarios in short time frames makes them invaluable.

5 Conclusion and Outlook

In this study, a newly developed electrolyzer model was presented and investigated under steady-state and dynamic operating conditions. The dynamic model was validated for steady-state operating and dynamic scenarios using measurement data.

First, the model was parametrized according to Crespi et al. (2023) and then unknown parameters were fitted to measurement data of the same publication. The fitted model agrees well with the measured polarization curve for three different operating temperatures. Next, the dynamic response of the electrolyzer model was adjusted by fitting the liquid mass and the gas volume of the fuel to measurement data. Again, a good agreement of the measurements and simulation is achieved. In both investigated operation points, the simulated stack temperatures match the measurements accurately. Furthermore, the pressure build-up in the cathode volume of the stack is predicted accurately by the simulation model.

In the last step, a dynamic load profile was generated based on real-world wind data. Two operating scenarios for the generated load profile were analyzed, one with and another without grid connection of the electrolyzer. The efficiency of grid-connected electrolyzer is higher than that of the standalone electrolyzer. The difference can be attributed to the operating phases with relatively low load, where the efficiency of hydrogen production is high. Furthermore, it was found that the hydrogen accumulation in the electrolyzer not connected to the grid is problematic in phases with low power supply. Finally, the degradation rate under dynamic load conditions was investigated, again using the load profile of the wind turbine. Here, an overprediction of the degradation rate by the implemented model was identified using the system simulation. In the future, more detailed degradation models, such as the one proposed in (Krenz et al. 2024), could be implemented.

Nomenclature

Abbreviations

MEA	Membrane Electrode Assembly
PEM	Proton Exchange Membrane
TSA	Temperature Swing Adsorption

Latin Symbols

A	Area, m^2
c	Concentration, $mol/(m^3)$
C	Heat capacity, J/K
F	Faraday Constant, C/mol
G	Gibbs free energy, J
$\dot{G}$	Gibbs free energy flow rate, W
h	Specific enthalpy, J/kg
H	Enthalpy J
$\dot{H}$	Enthalpy flow W
i	Current Density, A/cm^2
I	Current, A
M	Molar mass, kg/mol
n	Number, *dimensionless*
$\dot{m}$	Mass flow rate, kg/s
$\dot{n}$	Molar flow rate, mol/s
p	Pressure, Pa
P	Power, W
$\dot{Q}$	Heat Flow Rate, W
R	Heat transfer resistance, K/W
S	Entropy, J/K
$\dot{S}$	Entropy Flow Rate, W/K
t	Time, s
T	Temperature, K
V	Volume, m^3
U	Voltage, V
z	Number of electrons

Greek Symbols

α	Heat transfer coefficient, $W/(m^2K)$
α	charge transfer coefficient
β	Mass transfer coefficient, m/s
δ	Thickness, m
ε	Void Fraction
ε	Electro-osmotic Drag Coefficient
η	Efficiency
λ	Water Content mol/mol
ξ	Mass fraction, kg/kg
ρ	Density, kg/m^3
σ	Proton Conductivity, S/m

Subscript

act	Activation
conc	Concentration
deg	Degradation
eff	Effective
g	Gas
H_2	Hydrogen
H_2O	Water
is	Isentropic
l	Liquid
L	Limit
mem	Membrane
O_2	Oxygen
perm	Permeation
R	Reaction
rev	Reversible
sat	Saturation
TN	Thermoneutral
x	Crossover

References

Ahluwalia, R.K. and X. Wang (2007-09). "Buildup of nitrogen in direct hydrogen polymer-electrolyte fuel cell stacks". en. In: *Journal of Power Sources* 171.1, pp. 63–71. ISSN: 03787753. DOI: 10.1016/j.jpowsour.2007.01.032.

Bernt, Maximilian Philipp (2019). "Analysis of Voltage Losses and Degradation Phenomena in PEM Water Electrolyzers". PhD thesis. Technische Universität München.

Crespi, Elena et al. (2023-02). "Experimental and theoretical evaluation of a 60 kW PEM electrolysis system for flexible dynamic operation". en. In: *Energy Conversion and Management* 277, p. 116622. ISSN: 01968904. DOI: 10.1016/j.enconman.2022.116622.

Dassault Systèmes SE (2024). *Dymola 2024x*. https://www.3ds.com/products-services/catia/products/dymola/.

Engel, Franziska K. et al. (2025-04). "Dynamic multi-physics 1D-model of a proton exchange membrane electrolysis cell". en. In: *International Journal of Hydrogen Energy* 119, pp. 56–72. ISSN: 03603199. DOI: 10.1016/j.ijhydene.2025.03.116.

German Meteorological Service (DWD) (2025). *Climate Data Centers*. https://opendata.dwd.de/.

Hancke, Ragnhild, Thomas Holm, and Øystein Ulleberg (2022-06). "The case for high-pressure PEM water electrolysis". en. In: *Energy Conversion and Management* 261, p. 115642. ISSN: 01968904. DOI: 10.1016/j.enconman.2022.115642.

Heier, Siegfried (2022). *Windkraftanlagen: Systemauslegung, Netzintegration und Regelung*. de. Wiesbaden: Springer Fachmedien Wiesbaden. ISBN: 978-3-658-36569-1 978-3-658-36570-7. DOI: 10.1007/978-3-658-36570-7. URL: https://link.springer.com/10.1007/978-3-658-36570-7.

Hou, Junbo and Min Yang (2024-06). *Green Hydrogen Production by Water Electrolysis*. en. 1st ed. Boca Raton: CRC Press. ISBN: 978-1-00-336893-9. DOI: 10.1201/9781003368939.

Klan, Herbert and André Thess (2013). "F2 Wärmeübertragung durch freie Konvektion: Außenströmung". In: *VDI-Wärmeatlas*. Berlin, Heidelberg: Springer Berlin Heidelberg, pp. 757–764. ISBN: 978-3-642-19981-3. DOI: 10.1007/978-3-642-19981-3_38.

Krenz, Tobias et al. (2024-12). "Reversible Degradation Phenomenon in PEMWE Cells: An Experimental and Modeling Study". en. In: *Journal of The Electrochemical Society* 171.12, p. 124501. ISSN: 0013-4651, 1945-7111. DOI: 10.1149/1945-7111/ad96e4.

Ma, Zhiwen et al. (2021-05). "A comprehensive modeling method for proton exchange membrane electrolyzer development". en. In: *International Journal of Hydrogen Energy* 46.34, pp. 17627–17643. ISSN: 03603199. DOI: 10.1016/j.ijhydene.2021.02.170.

Rakousky, Christoph (2016). "Langzeitstabilität der Polymerelektrolyt-Wasserelektrolyse bei reduziertem Iridiumgehalt". Dissertation. Rheinisch-Westfälische Technische Hochschule Aachen.

Reimann, Ansgar, Paul Kohlenbach, and Lars Röntzsch (2023-12). "Development of a novel quasi-2D PEM Electrolyzer Model in Modelica". en. In: pp. 63–72. DOI: 10.3384/ecp20463.

Richter, Christoph (2008-04). "Proposal of New Object-Oriented Equation-Based Model Libraries for Thermodynamic Systems". PhD thesis. Technische Universität Braunschweig. DOI: 10.24355/dbbs.084-200806100200-3.

Schofield, Landon et al. (2025-01). "Dynamic optimization of proton exchange membrane water electrolyzers considering usage-based degradation". en. In: *AIChE Journal* 71.1, e18635. ISSN: 0001-1541, 1547-5905. DOI: 10.1002/aic.18635.

Springer, T. E., T. A. Zawodzinski, and S. Gottesfeld (1991-08). "Polymer Electrolyte Fuel Cell Model". en. In: *Journal of The Electrochemical Society* 138.8, pp. 2334–2342. ISSN: 0013-4651, 1945-7111. DOI: 10.1149/1.2085971.

Struchtrup, Henning (2014). *Thermodynamics and energy conversion*. Springer.

Tang, Tian (2016). "Analyse der Energieeffizienz eines Brennstoffzellenstapels im Kaltstartbetrieb". PhD thesis. Technische Universität Braunschweig.

Tjarks, Geert (2017). *PEM-Elektrolyse-Systeme zur Anwendung in Power-to-Gas Anlagen*. de. Jülich: Forschungszentrum Jülich GmbH, Zentralbibliothek. ISBN: 978-3-95806-217-7.

Tjarks, Geert et al. (2018-05). "Energetically-optimal PEM electrolyzer pressure in power-to-gas plants". en. In: *Applied Energy* 218, pp. 192–198. ISSN: 03062619. DOI: 10.1016/j.apenergy.2018.02.155.

TLK Energy GmbH (2024). *TIL Adsorption*. https://https://tlk-energy.de/en/software/til-suite/adsorption.

TLK-Thermo GmbH (2024). *TIL Suite*. https://www.tlk-thermo.com/en/software/til-suite.